Microgravity Science and Technology (2022) 34: 66
https://doi.org/10.1007/s12217-022-09976-x

ORIGINAL ARTICLE

Thermocapillary-buoyancy Convection Driven by a Horizontal Temperature Gradient in a Thin Liquid Layer: The Effect of Evaporation

Jun Qin[1,2] · Qiu-Sheng Liu[1,2] · Yue-Qun Tao[1] · Li-Li Qiao[1,2] · Zhi-Qiang Zhu[1]

Received: 16 March 2022 / Accepted: 21 June 2022 / Published online: 25 July 2022

Abstract

The effects of phase change on the stability of a horizontally heated liquid layer are studied experimentally in this paper. Results are obtained for two volatile liquids with similar Prandtl numbers in a rectangular geometry with different temperature differences. Three different flow states occur with the variation of the liquid depth, namely oscillating multicellular convection, hydrothermal waves and steady flow. The critical conditions for the transition between the different flow states are identified and discussed. In addition, the presence of evaporation at the interface plays an essential role in the flow instabilities. The results show that evaporation at the surface and associated surface deformation tend to inhibit the development of a hydrothermal wave but conversely promote the transition of oscillating multicellular convection. Furthermore, the transient nature of HTWs is shown to be little affected by the phase change.

Keywords Thermocapillary-buoyancy convection · Evaporation · Flow instability and transition

Introduction

Thermocapillary buoyancy convection plays a significant role in scientific and industrial fields, such as crystal growth, thermal management devices, and heat pipe technology. Numerous studies on thermocapillary flow have been carried out through theoretical analysis, experimental investigation, and numerical simulation. The first experimental study of thermocapillary convection began in 1978, Schwabe et al. (1978) confirmed the existence of thermocapillary instabilities in experiments on surface-tension-driven flow in floating zone melting. In 1982, Smith and Davis (1983) systematically investigated, on the basis of earlier experimental observations, the instability of thermocapillary convection generated by a constant horizontal temperature difference in an infinite plane fluid layer with a free top surface. They found a new form of instability which they termed a hydrothermal wave (hereafter referred to as HTWs). This different mode is a temperature perturbation wave that propagates in a direction that depends on the Prandtl number of the liquid. For moderate Pr, the waves are predicted to propagate obliquely upstream with a propagation angle against the surface flow. This behavior is consistent with the experimental results presented in this paper.

Subsequently, an increasing number of studies related to the thermocapillary-buoyancy convection in rectangular geometries have been performed by experimental measurements and numerical simulations. Riley and Neitzel (1998) observed and confirmed a pure hydrothermal-wave instability in shallow layers for 1cSt oil. They pointed out that the transition of HTWs was observed only for sufficiently thin layers, and that another instability which they termed oscillatory multicellular convection (hereafter referred to as OMC) is present for thicker layers. Burguete et al. (2001) studied the buoyant-thermocapillary convection in a rectangular geometry with different aspect ratios and found two types of wave sources as a function of fluid depth. Xu and Zebib (1998) performed 2D and 3D numerical investigations on rectangular cavities for fluids with $1 \leq Pr \leq 13.9$ and delineated the bifurcation neutral curves. Bucchignani (2004) numerically investigated the characterization of

This article is part of the Topical Collection on *The Effect of Gravity on Non-equilibrium Processes in Fluids*
Guest Editors: Tatyana Lyubimova, Valentina Shevtsova

✉ Qiu-Sheng Liu
liu@imech.ac.cn

[1] Institute of Mechanics, Chinese Academy of Sciences, 100190 Beijing, China

[2] University of Chinese Academy of Sciences, 100049 Beijing, China

hydrothermal waves based on the experiments of Riley and Neitzel (1998). Their results of oscillatory temperature and velocity perturbations were consistent with the observation of pure HTWs.

However, as mentioned before, these studies assumed that the free surface was adiabatic and ignored the effect of surface evaporation. Since evaporation occurs at the free surface of the liquid layer, the flow can become unstable even without a horizontal thermal gradient. Chai and Zhang (1998) and Zhang and Chao (1999) conducted previous research on thermocapillary-buoyancy convection with evaporation. They investigated the convection mechanisms of instability by a series of experiments in thin liquid layers. Then, Zhu et al. (2009) experimentally investigated the effects of evaporation on thermocapillary convection in a thin liquid layer. Their results showed that evaporation adversely affects the temperature gradient compared to thermocapillary convection. Moreover, by validating the experimental results of Zhu and Liu (2010), Sáenz et al. (2013, 2014) developed and proposed a new phase-change model to study the effects of phase change and interfacial deformation on the laterally heated liquid layer in a rectangular pool open to the atmosphere. Their work shows that the phase change plays a dual role through its effect on flow instabilities: the surface evaporation tends to inhibit the HTWs, while the accompanying level reduction enhances the physical waves by minimizing the role of gravity. To investigate the effects of the gas layer, Li et al. (2014) conducted a series of experiments with a volatile binary-fluid mixture in a confined cavity under non-condensable gasses. They observed four distinct flow regimes by changing the air concentration and gas pressure. These regimes are the result of the combined effects of thermal capillarity, solute capillarity, and buoyancy. Based on the experimental results of Li et al. (2014), Qin et al. (2014) and Qin (2017) numerically studied the combined evaporation effect and thermocapillary convection in a sealed rectangular cavity using a two-sided model with phase change. They found that non-condensable gasses play a significant role in the transitions between different flow patterns and heat and mass transfer at the interface through their effects on the evaporation rate. Xu et al. (2020) further developed the earlier two-sided model to account for the phase-change effect on the thermocapillary-buoyancy convection in a closed cavity. Their work reveals a new feature of flow instability coupled with the phase change effect and confirms the stabilizing effect of evaporation on the thermocapillary-buoyancy convection.

As mentioned above, few experimental studies of thermocapillary-buoyancy convection have considered the effects of surface evaporation and, most importantly, have provided further details on the evolution of different flow patterns. In this study, we report a series of experimental results on thermocapillary-buoyancy convection in an open cavity subjected to various temperature differences. Two types of fluids with moderate-Prandtl-number (0.65cSt oil and HFE7200) were chosen as working fluids because they have similar Pr number but different saturation vapor pressure. This article focuses on the evolution of the flow state and provides a preliminary analysis of the effects of surface evaporation on the properties of the flow state.

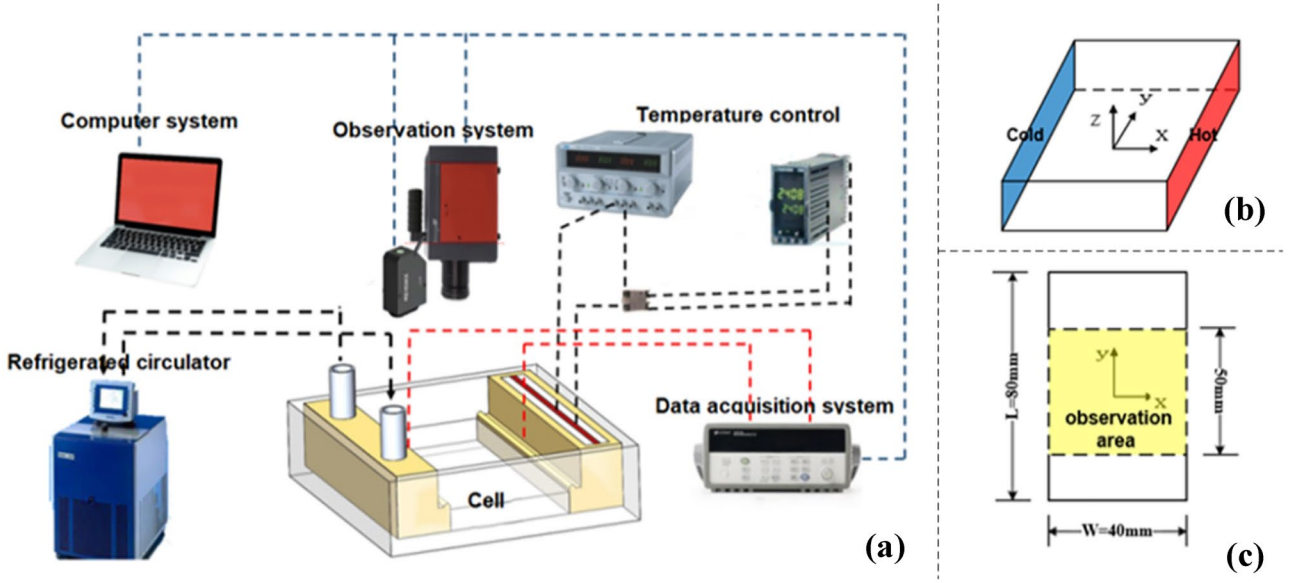

Fig. 1 Schematic drawing of the experimental apparatus

Table 1 Physical properties of 0.65cSt silicone oil and HFE7200 at 25℃

	$\rho_L[kg/m^3]$	$\mu[Pa \bullet s]$	σ[N/m]	$\alpha[m^2/s]$	Pr	$\beta[K^{-1}]$	$\sigma_T[N/(m \bullet K)]$	$P_{sat}[kPa]$
0.65cSt oil	760	4.95×10^{-4}	0.0159	6.3×10^{-8}	10.3	0.00134	8×10^{-5}	4.7
HFE7200	1430	5.7×10^{-4}	0.0136	3.7×10^{-8}	10.1	0.00158	9×10^{-5}	16

Experimental Setup and Method

The entire experimental setup is shown in Fig. 1. The test cell's length L and width W are 80 mm and 40 mm, respectively. The two longer sidewalls of the cavity are made of copper with good thermal conductivity for temperature control. The temperature control of hot sidewall is done by PID loops with a thermoelectric Peltier device, which has an accuracy of 0.05 °C . For the temperature control of the cold side, a refrigerated circulator with cool water of constant temperature is fed into the cold sidewall, and the accuracy could be 0.02 °C. Two thermocouples, mounted in the middle of the two copper walls, directly measure the temperature of the sidewall. The bottom and the two shorter sides of the flow cell are made of Plexiglas, which is considered to be adiabatic. The top of the cavity is open to the atmosphere, allowing the liquid to evaporate freely.

To achieve an accurate measurement of the depth d and its continuous variability, a laser co-focal displacement meter is used to detect the position of the liquid-vapor interface with an accuracy of 0.3μm. At the beginning of experiments, a centering reference surface is placed at the bottom of the cell so that we can record the instantaneous depth of the working liquid during the evaporation process. Meanwhile, a rounded lip was milled along the inner sides of the copper to eliminate the meniscus at the boundaries.

The temperature distribution and fluctuation on the free surface is observed using the infrared thermography technique, which is central to the determination of flow states encountered in this work. These measurements are made with an infrared(IR) camera(ImageIR 8300) that uses a 128× 128 element indium-antimonide focal-plane-array detector, sensitive to radiation in the range of 2–5μm. Infrared images are acquired at a speed of 8 fps with a resolution of 640× 512 pixels. This instrument facilitates the study of oblique hydrothermal-wave instabilities and other flow regimes. It also allows observation of the continuous transition between different flow regimes and flow structures. Due to the limited visibility of infrared field, the actual observation area can be seen in Fig. 1c. In the meantime, we set up a coordinate system in this flow model, as shown in Fig. 1b, which is suitable for spatiotemporal evolution analysis. The whole experimental setup is placed on a vibration-isolated platform and is mantled with a glass cover to avoid interference from the surrounding environment. The ambient temperature outside the glass cover is 25 °C.

The working fluids used in these experiments are 0.65cSt oil and HFE7200, which are relatively resistant to contamination. Meanwhile, both fluids have relatively high saturated vapor pressure, so they evaporate quickly under atmospheric conditions. The physical properties are listed in Table 1. Note that the P_{sat} values of the two liquids given here are quite different, resulting in different evaporation rates. At the beginning of the experiment, a 2.1 mm deep layer of liquid is injected into the cavity from above after a stable temperature difference is established. Then, we observe the flow state until the liquid dries out. In these cases, the corresponding temperature and interface changes can be recorded.

Results and Discussion

Average Evaporating Rate

To evaluate the effects of evaporation, we choose the average evaporation rate as a quantitative index. Given that the evaporation rate is different at different positions, we choose the evaporation rate in the center of the cavity as the overall average evaporation rate. The average evaporation rate of the liquid layer is defined as follows,

$$E = \frac{\partial H}{\partial t} \tag{1}$$

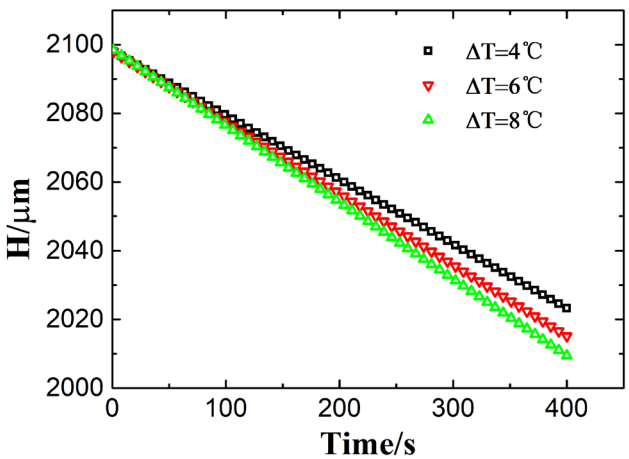

Fig. 2 Variation of the 0.65cSt silicone oil layers thickness with the evaporating time

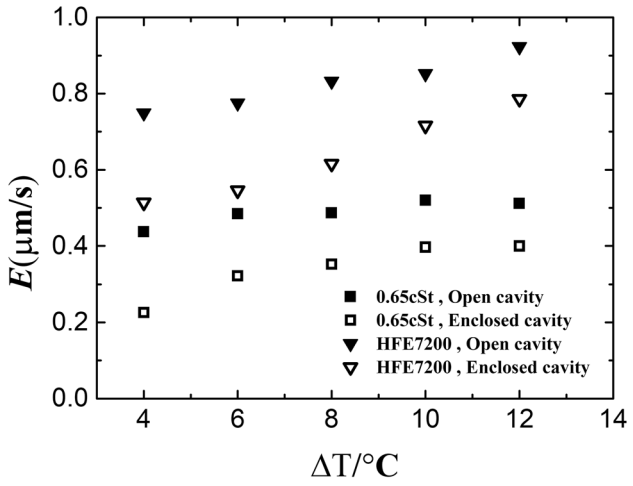

Fig. 3 Average evaporating rates for the different temperature differences

We measured the variation of the interfacial height at different temperature differences. Figure 2 shows some measurement results of the variation of the interfacial height over a period of time at three groups of temperature differences for 0.65cSt silicone oil layers. It is clear that the depth of the liquid layer decreases linearly with evaporation time, and the height variation of the interface is much smaller in magnitude than the decrease of the liquid depth during the evaporation process. Therefore, it is applicable and reasonable to use formula (1) to define the average evaporation rate in our experiment. Eventually, the average evaporation rate is calculated by linear approximation to the height variation.

In these experiments, we conducted two sets of evaporation experiments under different conditions. First, the rectangular pool is open to the environment, and second, the pool is covered with a plexiglass over the liquid layer to slow down the evaporation. These two sets of comparative experiments enable us to study the evaporation effect on thermocapillary-buoyancy convection at the same temperature difference individually, eliminating the effects caused by temperature variations.

Figure 3 shows the average evaporation rates of 0.65cSt oil and HFE7200 at different temperature differences under both open cavity and closed cavity conditions. As the temperature difference increases, the average evaporation rate increases monotonously, while the difference in average evaporation rate between these two conditions decreases for each liquid. This means that the gas phase has less influence on evaporation at higher temperature differences. Meanwhile, the average evaporation rate of HFE7200 is about twice that of 0.65cSt oil at the same temperature difference, which is conducive to the analysis of the evaporation effect on flow stability.

Observed Flow Regimes

Once $\Delta T \neq 0$ is reached, thermocapillary-buoyancy convection occurs. The thermal gradient along the interface creates a surface tension gradient, that causes surface flow from the hot side to the cold side, with recirculation at the bottom. Buoyancy forces can also affect the flow. To suppress the buoyancy effect, the initial depth of the liquid layer is kept smaller than 2.0 mm, which corresponds to a Bond number of 0.55. Depending on the temperature difference and layer thickness, the flow can destabilize into different patterns. In this study, the flow transition path is oscillating multicellular convection (OMC) → hydrothermal wave (HTW) → basic flow (BF) throughout the evaporation process. In the following, we first introduce the oscillating multicellular convection and then the different flow regimes.

Oscillating Multicellular Convection

The free-surface thermography of this flow is shown in Figs. 4a and 5a. For the 0.65cSt silicone oil liquid layers, a chevron pattern resembling two interacting traveling waves is observed throughout the cell. The multicellular structure spreads across the cold and hot sides of the thermograph like the net. However, unlike the 0.65cSt silicone oil liquid layer, only a few structures can be seen near the cold side of the

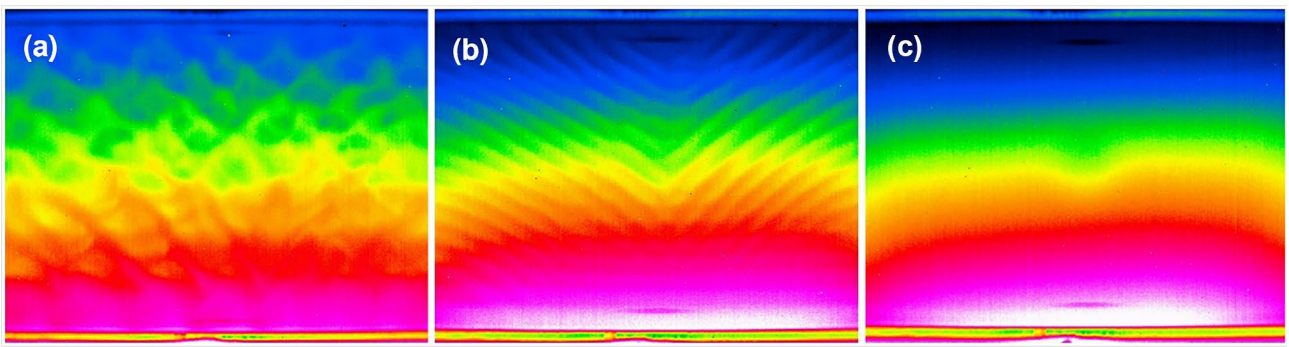

Fig. 4 ΔT = 6.0 °C, three kinds of observed IR thermal patterns of 0.65cSt silicone oil liquid layers during the evaporation process

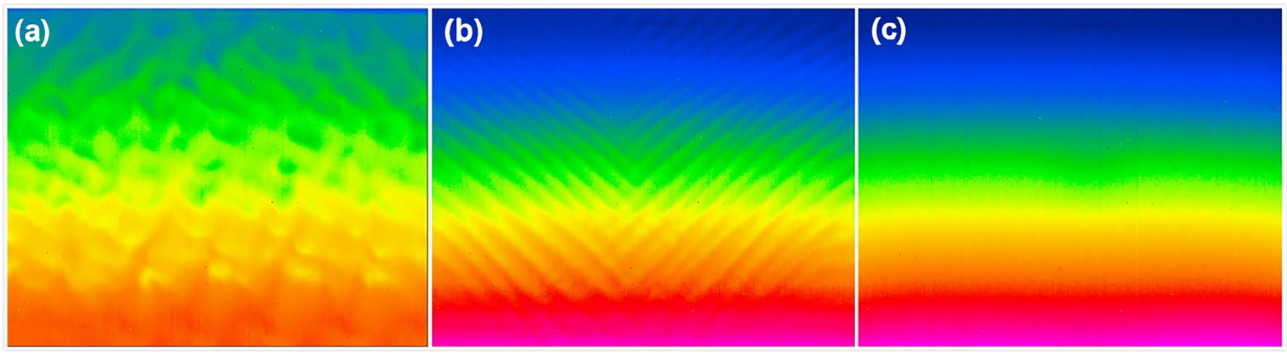

Fig. 5 $\Delta T = 6.0$ °C, three kinds of observed IR thermal patterns of HFE7200 liquid layers during the evaporation process

evaporating HFE7200 liquid layer. Only in the hot region, there are still some similar net structures. In these cases, the flow states observed here all propagate thermal fluctuations about the base state. Thus, to analyze their transient characteristics, the local value of the temperature fluctuation T' on the free surface separated from the base state is introduced as follows

$$T' = T - \frac{1}{L}\int_{-\frac{L}{2}}^{+\frac{L}{2}} T\, dy$$

which is a better representation of the thermal perturbation.

Figures 6, 7 and 8 show the overall OMC development with time using the spatial-time diagrams of surface temperature fluctuation T' with different directions for different evaporation layers. Obviously, for the 0.65cSt silicone oil liquid layers, a bundle of oblique waves has emerged, propagating from the cold side toward the hot side in the streamwise direction, as shown in Fig. 6a. Meanwhile, there remain strong oscillating multicellular structures near the cold side seen in Fig. 7a. Figure 7b, c show the subsequent evolution of OMC in the spanwise direction. In the central position of the cavity, there are almost no distinct multicellular structures while a pair of traveling waves forms until the end of the cell. Therefore, the overall development of OMC is that the initial oscillating cells gradually move and develop into two traveling waves in opposite directions. In liquid layers with faster evaporation, here the HFE7200 liquid layers, the evolution of OMC shows a different behavior. In the cold region, a chaotic pattern seems to initiate the whole flow and no similar structures are found compared to the previous layers, as shown in Fig. 8a. It could be that the stronger evaporation disrupts the temperature distribution at the interface, leading to larger temperature fluctuations and the absence of convective cells. But a small number of ripples and reticular structures can also be observed. And in the main area, a visible wave develops with time, as can be seen in Fig. 8b, c. In fact, the oscillatory state observed here is not a pure traveling-wave state, but rather a traveling wave superimposed on steady corotating rolls.

Riley and Neitzel (1998) observed a similar experimental result in a rectangular domain, but they did not give a detailed evolution process of this flow state in different positions. They state that this flow pattern is derived from a steady multicellular flow, and steady multi cells are still established at the hot wall. However, in this study, it is not a steady multicellular structure near the hot side but a pair of traveling waves.

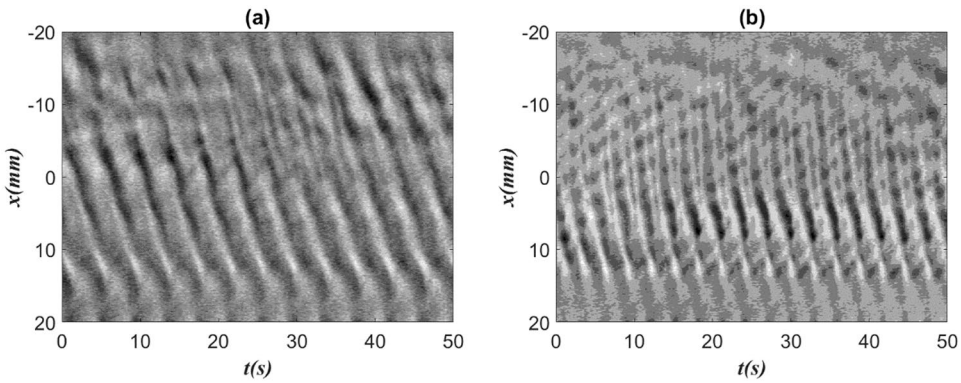

Fig. 6 Space-time diagrams for T' along the central streamwise section for **a** the 0.65cSt silicone oil liquid layers and **b** the HFE7200 liquid layers

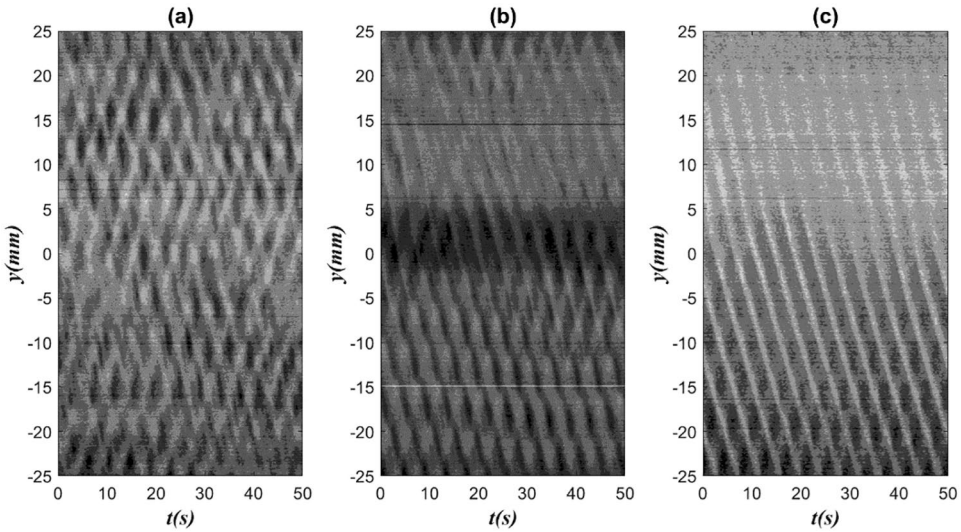

Fig. 7 Space-time diagrams for T' along the spanwise section at **a** x=-15 mm **b** $x=0$ mm **c** $x=15$ mm for the 0.65cSt silicone oil liquid layers

Hydrothermal Waves

If the liquid layer continues to evaporate, a hydrothermal-wave transition occurs at low layer thickness. The transition between these two flow states is not sharp. Two interacting traveling waves, as mentioned above, always approach a line in the center of the cavity, and then propagate separately in the opposite direction. These HTWs are traveling thermal waves, that propagate obliquely at the moderate Prandtl number of the liquid used in these experiments. Figures 4b and 5b show the instantaneous thermographs of the HTWs. It is clear that a pair of waves, propagating obliquely in opposite directions from the cold side to the hot side, fill the cavity. The waves are separated by a source, that looks like a point located on the cold wall and emits a V-shaped wave.

Figures 9 and 10 show the general HTW evolution with time using the spatial-time diagrams of the surface temperature fluctuation T' along with different directions for different evaporation layers. It is clear that a single oblique wave moves with time toward the hot wall for both 0.65cSt silicone and HFE7200 liquid layers, as shown in Figs. 9a and 10a. The difference with the waves in the latter case is that they are less intact and disappear at the sidewalls. This is probably the reason that more evaporation leads to a weakening of the temperature fluctuations. Note that the wave pattern in these two figures is less pronounced on the hot side, which is actually due to the presence of a single steady rolling cell on the hot wall. This is also consistent with the experimental observations and numerical simulations of Riley and Neitzel (1998) and Xu et al. (2020). In the spanwise direction,

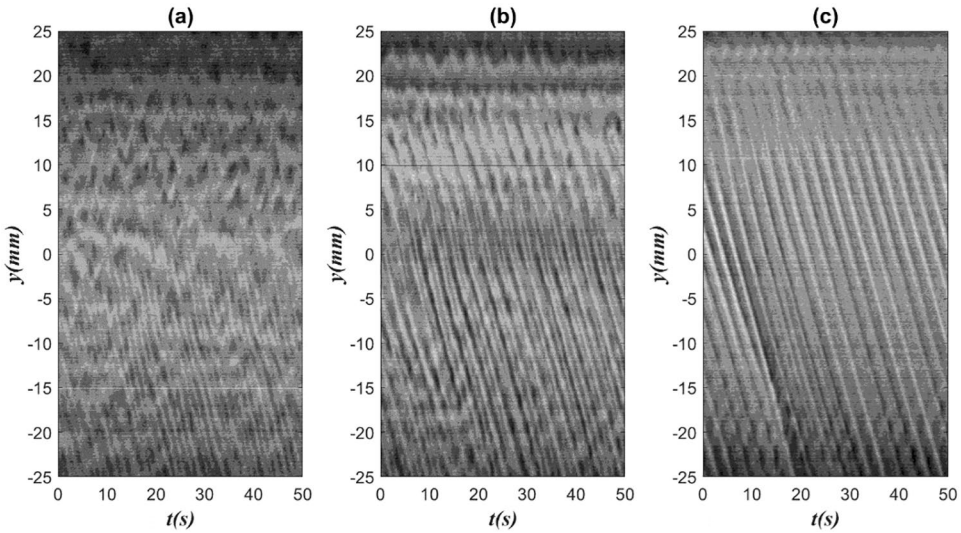

Fig. 8 Space-time diagrams for T' along the spanwise section at **a** x=-15 mm **b** $x=0$ mm **c** $x=15$ mm for the HFE7200 liquid layers

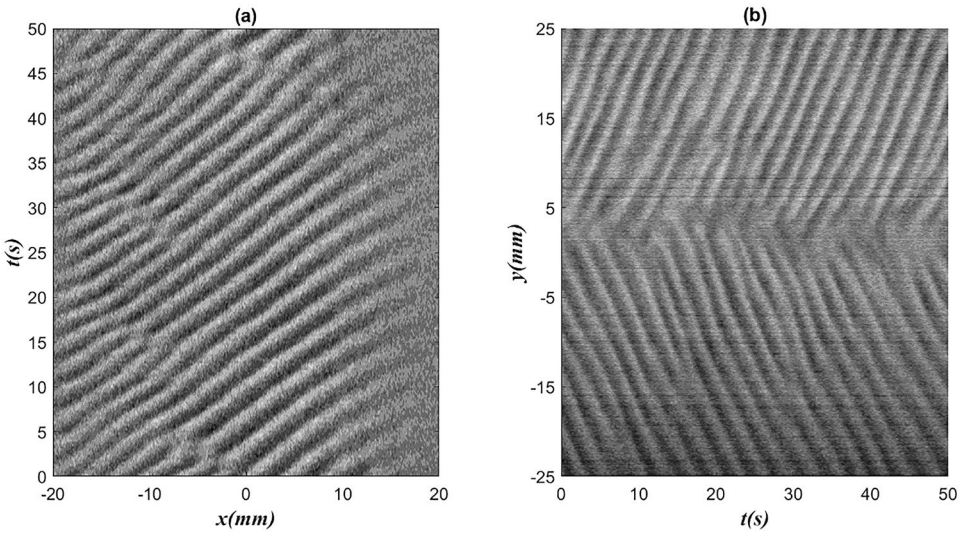

Fig. 9 Space-time diagrams for T' along the central streamwise section (left) and the spanwise section at x=-15 mm (right) for the 0.65cSt silicone oil liquid layers

both evolutions are the same and are consistent with thermography (Figs. 9b and 10b).

Characteristics of the HTWs

The characteristics of the waves are quantified in terms of wavenumber k, and the angle of propagation Ψ, which are extracted from the infrared images of the interface temperature fields. Dimensional values of these quantities at different values of ΔT are presented in Table 2. It shows the evolution of the different features of the HTWs in the evaporation process for the different temperature differences. For the same temperature difference, the wavenumber tends to increase with evaporation while the propagation angle remains approximately constant. This means that the liquid-level reduction caused by the evaporation enhances the HTWs. As the layer becomes thinner, the reduced buoyancy effect mitigates the inhibitory effect on the thermocapillary convection. However, the evaporation does not appear to directly affect the feature of the HTWs. For instance, the wavenumber remains nearly constant when H is the same between different ΔT of 4 and 6. Another characteristic, referred to as the propagation angle, is independent of ΔT and H and remains nearly unchanged. Note that the propagation angle is different for low values of ΔT. This is because the HTWs is not a symmetric wave when the ΔT is 4 °C and the propagation angle is different in a different direction.

Critical Condition of Flow Destabilization

In the present experiments, five different sets of temperature differences are applied to the sidewalls of the cavity,

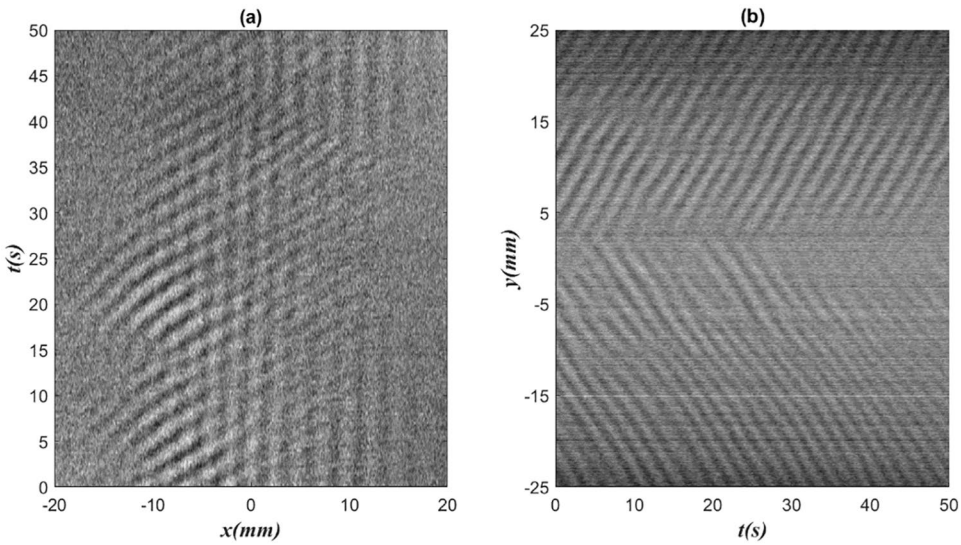

Fig. 10 Space-time diagrams for T' along the central streamwise section (left) and the spanwise section at x=-15 mm (right) for the HFE7200 liquid layers

Table 2 dimensional characteristics of the hydrothermal waves as a function of the layer depth at various ΔT for 0.65cSt oil silicone

ΔT = 4 °C			ΔT = 6 °C			ΔT = 10 °C		
H(mm)	$k(mm^{-1})$	Ψ°	H(mm)	$k(mm^{-1})$	Ψ°	H(mm)	$k(mm^{-1})$	Ψ°
1.49	0.22	119	1.2	0.38	138	1.09	0.47	144
1.37	0.30	121	1.11	0.45	139	0.97	0.51	140
1.25	0.34	125	1	0.52	136	0.85	0.59	140
1.2	0.38	127	0.89	0.52	141			

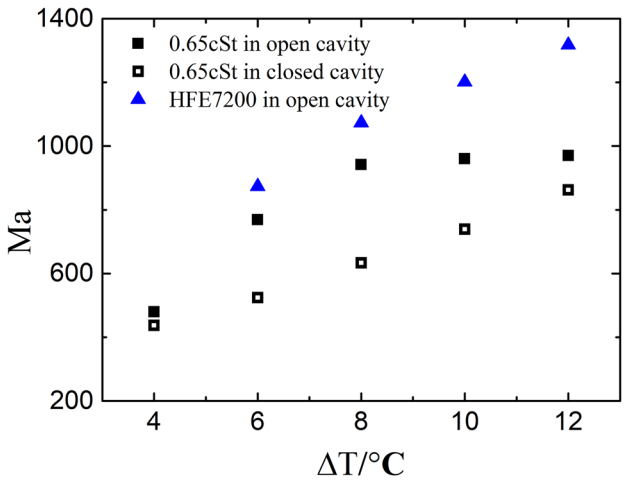

Fig. 11 Variation of the critical Marangoni number with the temperature difference

and observed until the end of evaporation, to obtain transient flow structure in the evaporation process. The flow states are mainly divided into three categories, as mentioned earlier. The results presented here will focus on the transition from the OMC to the HTWs. Figure 11 shows the variation of the transitional Marangoni number with different temperature differences for three types of experimental conditions, related to the different evaporation rates. It is evident that the critical Marangoni number increases with increasing evaporation, suggesting that evaporation suppresses the transition to the HTWs and indirectly promotes the generation of the OMC. Another point is that there is actually an additional Marangoni number to characterize the transition from the HTWs to a steady flow. Nevertheless, the thickness corresponding to the OMC is so tiny that the fluid can be considered as a liquid film rather than a liquid layer.

Conclusions

The effect of evaporation on the thermocapillary-buoyancy convection of two types of volatile liquids driven by different horizontal temperature differences is studied experimentally through different measurements. In the presence of evaporation, the flow is more complicated and exhibits some new phenomena.

The flow is classified into three distinct flow patterns, namely oscillating multicellular convection (OMC), hydrothermal wave (HTW), and steady flow (SF). In the OMC, a bunch of oblique traveling waves fills the whole domain and propagates from the cold side towards the hot side in the streamwise direction. It originates on the cold side and gradually evolves towards the hot side. As time goes on, two waves join together and form a net structure through the cavity. For the liquid layer with stronger evaporation, the effect of phase change is mainly on the cold side, which destroys the thermal gradient along the interface and induces more intense temperature fluctuations. And in the HTWs, the transition is observed when the liquid layer is sufficiently thin. At the surface, this flow pattern resembles a pair of oblique traveling waves separated by a line along the flow direction, propagating from the cold side to the hot side. And no significant differences in the flow pattern are seen between the two cases with different evaporation rates.

As the evaporation progresses, due to the combined effect of buoyancy and thermal capillary force, the wavenumber of HTW gradually increases and the propagation angle remains at 140. Moreover, the evaporation plays a minor role in the expression of the waves when the magnitudes are compared at different temperature differences. On the other hand, the phase change plays a dual role in the transitions: it tends to inhibit the emergence of a hydrothermal wave but conversely promotes the transition of oscillating multicellular convection.

Acknowledgements This work was financially supported by the National Natural Science Foundation of China (Grants No. 11532015, No. 11302236), by the Strategic Priority Research Program on Space Science, Chinese Academy of Sciences (Grants No. XDA04073000, XDA04020202-02) and China Manned Space Program (TZ-1).

Declarations

Conflict of Interests The authors declare that there is no conflict of interest.

References

Bucchignani, E.: Numerical characterization of hydrothermal waves in a laterally heated shallow layer. Phys. Fluids. **16**, 3839–3849 (2004). https://doi.org/10.1063/1.1776963

Burguete, J., Mukolobwiez, N., Daviaud, F., Garnier, N., Chiffaudel, A.: Buoyant-thermocapillary instabilities in extended liquid layers subjected to a horizontal temperature gradient. Phys. Fluids. **13**, 2773–2787 (2001). https://doi.org/10.1063/1.1398536

Chai, A.T., Zhang, N.L.: Experimental study of Marangoni-Bénard convection in a liquid layer induced by evaporation. Exp. Heat Transf. **11**, 187–205 (1998). https://doi.org/10.1080/08916159808946561

Li, Y.R., Grigoriev, R., Yoda, M.: Experimental study of the effect of noncondensables on buoyancy-thermocapillary convection in a volatile low-viscosity silicone oil. Phys. Fluids. **26**, 122112 (2014). https://doi.org/10.1063/1.4904870

Qin, T.R.: Buoyancy-thermocapillary convection of volatile fluids in confined and sealed geometries. (2017). http://link.springer.com/10.1007/978-3-319-61331-4

Qin, T.R., Tuković, Z., Grigoriev, R.O.: Buoyancy-thermocapillary convection of volatile fluids under atmospheric conditions. Int. J. Heat Mass Transf. **75**, 284–301 (2014). https://doi.org/10.1016/j.ijheatmasstransfer.2014.03.027

Riley, R.J., Neitzel, G.P.: Instability of thermocapillary–buoyancy convection in shallow layers. Part 1. Characterization of steady and oscillatory instabilities. J. Fluid Mech. **359**, 143–164 (1998). https://doi.org/10.1017/S0022112097008343

Sáenz, P.J., Valluri, P., Sefiane, K., Karapetsas, G., Matar, O.K.: Linear and nonlinear stability of hydrothermal waves in planar liquid layers driven by thermocapillarity. Phys. Fluids. **25**, 094101 (2013). https://doi.org/10.1063/1.4819884

Sáenz, P.J., Valluri, P., Sefiane, K., Karapetsas, G., Matar, O.K.: On phase change in Marangoni-driven flows and its effects on the hydrothermal-wave instabilities. Phys. Fluids. **26**, 024114 (2014). https://doi.org/10.1063/1.4866770

Schwabe, D., Scharmann, A., Preisser, F., Oeder, R.: Experiments on surface tension driven flow in floating zone melting. J. Cryst. Growth. **43**, 305–312 (1978)

Smith, M.K., Davis, S.H.: Instabilities of dynamic thermocapillary liquid layers. Part 1. Convective instabilities. J. Fluid Mech. **132**, 119–144 (1983). https://doi.org/10.1017/S0022112083001512

Xu, G.F., Liu, Q.S., Qin, J., Zhu, Z.Q.: Numerical study of thermocapillary-buoyancy convection of volatile liquid layer in an enclosed cavity. Microgravity Sci. Technol. **32**, 305–319 (2020). https://doi.org/10.1007/s12217-019-09763-1

Xu, J.Y., Zebib, A.: Oscillatory two- and three-dimensional thermocapillary convection. J. Fluid Mech. **364**, 187–209 (1998). https://doi.org/10.1017/S0022112098001232

Zhang, N.L., Chao, D.F.: Mechanisms of convection instability in thin liquid layers induced by evaporation. Int. Commun. Heat Mass Transf. **26**, 1069–1080 (1999). https://doi.org/10.1016/S0735-1933(99)00098-6

Zhu, Z.Q., Liu, Q.S.: Coupling of thermocapillary convection and evaporation effect in a liquid layer when the evaporating interface is open to air. Chin. Sci. Bull. **55**, 233–238 (2010). https://doi.org/10.1007/s11434-009-0693-2

Zhu, Z.Q., Liu, Q.S., Xie, J.C.: Experimental study on the combined evaporation effect and thermocapillary convection in a thin liquid layer. Microgravity Sci. Technol. **21**, 241–246 (2009). https://doi.org/10.1007/s12217-009-9123-y